Mineralogical Magazine (2025), **89**, 535–543
doi:10.1180/mgm.2025.16

Article

Edwindavisite, $Cu(C_2O_4)(NH_3)$, a new oxalate mineral, from the Rowley mine, Maricopa County, Arizona, USA

Hexiong Yang[1], Xiangping Gu[2], Anthony R. Kampf[3], Joe Marty[3], Ronald B. Gibbs[1] and Robert T. Downs[1]

[1]Department of Geosciences, University of Arizona, Tucson, AZ, USA; [2]Guanghua School of Gems and Art Design, Jiangxi Institute of Applied Science and Technology, Nanchang, JX, China and [3]Mineral Sciences Department, Natural History Museum of Los Angeles County, Los Angeles, CA, USA

Abstract

A new oxalate mineral species, edwindavisite, ideally $Cu(C_2O_4)(NH_3)$, was discovered in specimens collected from the Rowley mine, Maricopa County, Arizona, USA. It occurs as fans or sprays of bladed or prismatic crystals (up to 0.50 × 0.08 × 0.06 mm), associated intimately with ammineite, a sampleite-like mineral, baryte, ebnerite, wulfenite and quartz. Edwindavisite is green, transparent with a pale green streak and has a vitreous lustre. It is brittle and has a Mohs hardness of ~2; cleavage is perfect on {100}. No parting or twinning was observed. The measured and calculated densities are 2.55(2) and 2.53 g/cm^3, respectively. Optically, edwindavisite is biaxial (+), with $\alpha = 1.550(2)$, $\beta = 1.559(2)$, $\gamma = 1.755(5)$, $2V_{meas.} = 26(2)°$ and $2V_{cal.} = 26.4°$. Electron microprobe analyses yielded the empirical formula (based on Cu = 1 apfu) $Cu_{1.00}(C_2O_4)(NH_3)_{0.99}$.

Edwindavisite is the natural counterpart of synthetic *catena*-μ-oxalato-ammine-copper(II), $Cu(C_2O_4)(NH_3)$. It is orthorhombic with space group *Pbca* and unit-cell parameters $a = 11.1998(10)$, $b = 9.4307(9)$, $c = 8.3977(7)$ Å, $V = 886.98(14)$ Å^3 and $Z = 8$. In the edwindavisite structure, each Cu^{2+} cation is coordinated by (5O + N), forming a rather distorted and elongated octahedron. The Cu-octahedra share corners with one another to form chains extending along [001], which are joined together by oxalate $(C_2O_4)^{2-}$ groups, giving rise to layers parallel to (100). These layers are linked together by N–H···O hydrogen bonds. Among 37 oxalate minerals documented to date, edwindavisite is the first one that contains ammonia (NH_3).

Keywords: edwindavisite; oxalate; ammonia; crystal structure; X-ray diffraction; Raman spectroscopy; bat guano; Rowley mine; Arizona

(Received 13 December 2024; revised 7 February 2025; accepted 8 February 2025; Accepted Manuscript published online: 27 February 2025)

Introduction

Oxalate minerals are the largest subclass of organic minerals. In the current list of minerals approved by the Commission on New Minerals, Nomenclature and Classification of the International Mineralogical Association (IMA-CNMNC, Pasero, 2025), those derived from organic acids include three acetates, one citrate, two formates, seven glycolates, one mellitate, one methanesulfonate and 37 oxalates. While some oxalate minerals may form abiotically, most are found to occur in connection with biological systems. They are known to form when sources of oxalic acid interact with metal cations leached from primary minerals (e.g. Baran and Monje, 2008; Baran, 2014; Frank-Kamenetskaya *et al.*, 2021). In biologically induced mineralisation, acid-producing microorganisms, such as fungi, lichens and bacteria, as well as guano, are common sources of oxalic acid (e.g. Baran, 2014; Gadd *et al.*, 2014). Moreover, oxalates represent the only ionic organic minerals known to be stable over geological timescales on Earth (Hoffman and Bernasconi, 1998; Hazen *et al.*, 2013). Thus, their presence may be an indicator of plant life either current or in pre-existing life forms.

Oxalate materials have been the subject of various investigations owing to their diverse applications, such as hydrogen storage, carbon sequestration, catalysis, gas separation and photovoltaics (e.g. de Faria *et al.*, 2007; Androš *et al.*, 2010; Furukawa *et al.*, 2013; Garcia-Teran *et al.*, 2019). In particular, the study of the crystallisation of copper oxalate is very interesting and promising, because copper is a toxic element and the formation of insoluble copper oxalate can be used in bioremediation technologies for copper-contaminated environments with the help of oxalate-producing microorganisms (e.g. Fomina *et al.*, 2005; Ren *et al.*, 2009; Tsekova *et al.*, 2010; Gadd *et al.*, 2014; Glukhova *et al.*, 2018). For example, Tsekova *et al.* (2010) described the recovery of copper and other metals from industrial wastewater using Aspergillus niger, which is one of the most commonly used oxalate-producing micromycetes (Gadd *et al.*, 2014; Zelenskaya *et al.*, 2021; Frank-Kamenetskaya *et al.*, 2022). Moreover, there have been numerous publications on the application of Cu-oxalates in industry for their

Corresponding author: Hexiong Yang; Email: hyang@arizona.edu
Associate Editor: Irina O Galuskina
Cite this article: Yang H., Gu X., Kampf A.R., Marty J., Gibbs R.B. and Downs R.T. (2025) Edwindavisite, $Cu(C_2O_4)(NH_3)$, a new oxalate mineral, from the Rowley mine, Maricopa County, Arizona, USA. *Mineralogical Magazine* **89**, 535–543. https://doi.org/10.1180/mgm.2025.16

Figure 1. A specimen (R230005) on which the new mineral edwindavisite (indicated by red arrows), was found.

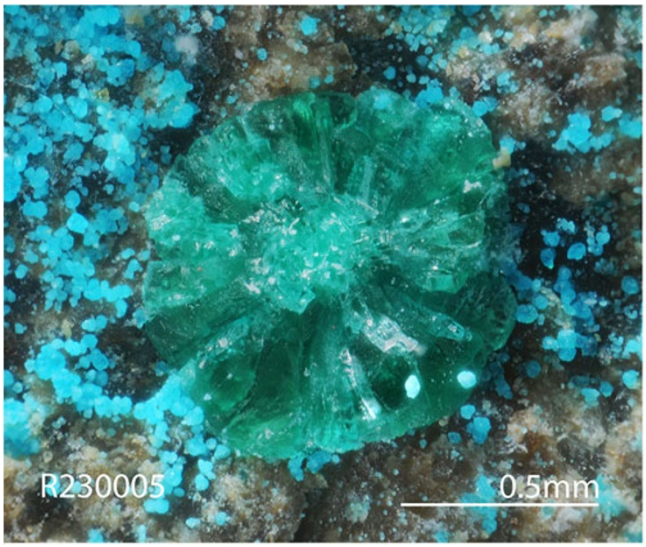

Figure 2. A microscopic view of Fig. 1 showing fans of green bladed edwindavisite crystals, associated with a blue sampleite-like phase and ammineite.

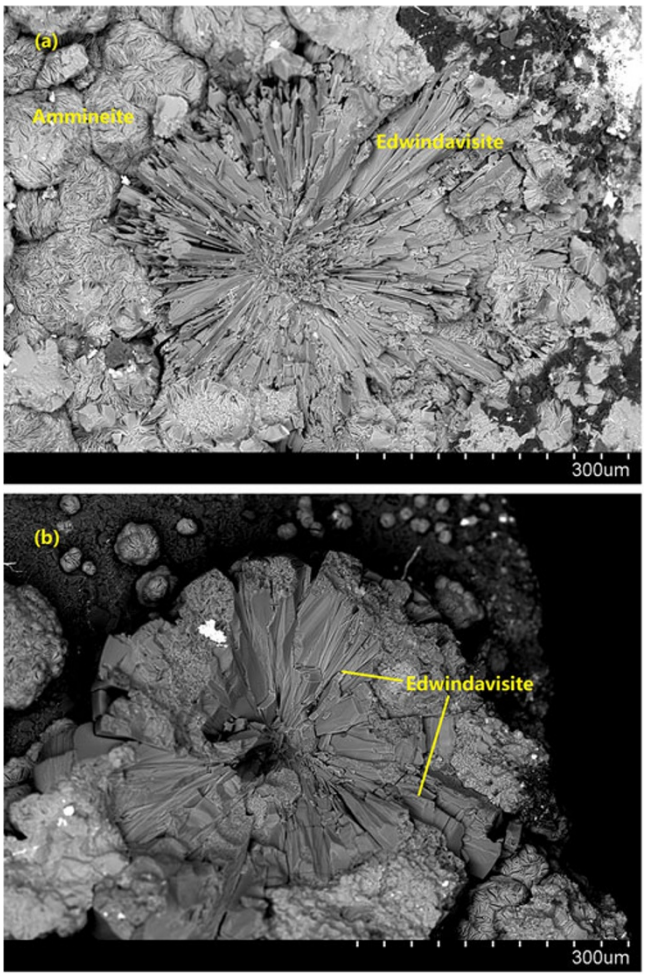

Figure 3. Back-scattered electron images (a and b), showing fans of prismatic or bladed edwindavisite crystals.

Table 1. Analytical chemical data (in wt.%) for edwindavisite

Const.	Mean	Min.	Max.	S.D.	Probe standard
NH_3	10.10	9.36	10.91	0.57	BN
C_2O_3	42.72				Added as ideal value
CuO	47.81	47.13	48.66	0.58	Cu_2O
Total	100.64	100.19	101.11	0.35	

interesting physical and chemical properties, including use as antiferromagnets (e.g. Donkova and Mehandjiev, 2005; Behnoudnia and Dehghani, 2013), and for their acting as a precursors to the formation of a number of widely used nanoparticles, such as Cu, CuO, Cu_2O and $Cu(OH)_2$ (e.g. Aimable *et al.*, 2011; Singh *et al.*, 2012; Gadd *et al.*, 2014; Wu and Huang, 2016).

This study describes a new oxalate mineral, edwindavisite, ideally $Cu(C_2O_4)(NH_3)$, discovered from the Rowley mine, Maricopa County, Arizona, USA. The new mineral name honours Mr. F. Edwin (Ed) Davis, Jr., an Arizona-based mineral collector and the current contractor operator of the Rowley mine, who has gladly accepted the proposed mineral name. Ed Davis graduated from Miami University in Oxford, Ohio, USA, with degrees in chemical engineering, mathematics and chemistry. He is credited for the discovery of the Purple Passion deposit near Wickenburg, Arizona, USA, which is world-renowned among fluorescent mineral collectors. Ed Davis has helped in the collection of multiple new minerals from the Rowley mine, such as ebnerite and epiebnerite (Kampf *et al.*, 2024), as well as edwindavisite described here. In particular, he provided access to the mine, helped in exploration, and helped in removing specimens from difficult to negotiate underground workings. The new mineral and its name (symbol Ewd) have been approved by the IMA (IMA 2023-056, Yang *et al.*, 2023). Parts of the cotype samples have been deposited at the University of Arizona Alfie Norville Gem and Mineral Museum (Catalogue # 22732) and the RRUFF Project (deposition # R230003). In addition, two cotype specimens are deposited in the collections of the Natural History Museum of Los Angeles County, Los Angeles, California, USA (catalogue numbers 76287 and 76288).

https://doi.org/10.1180/mgm.2025.16 Published online by Cambridge University Press

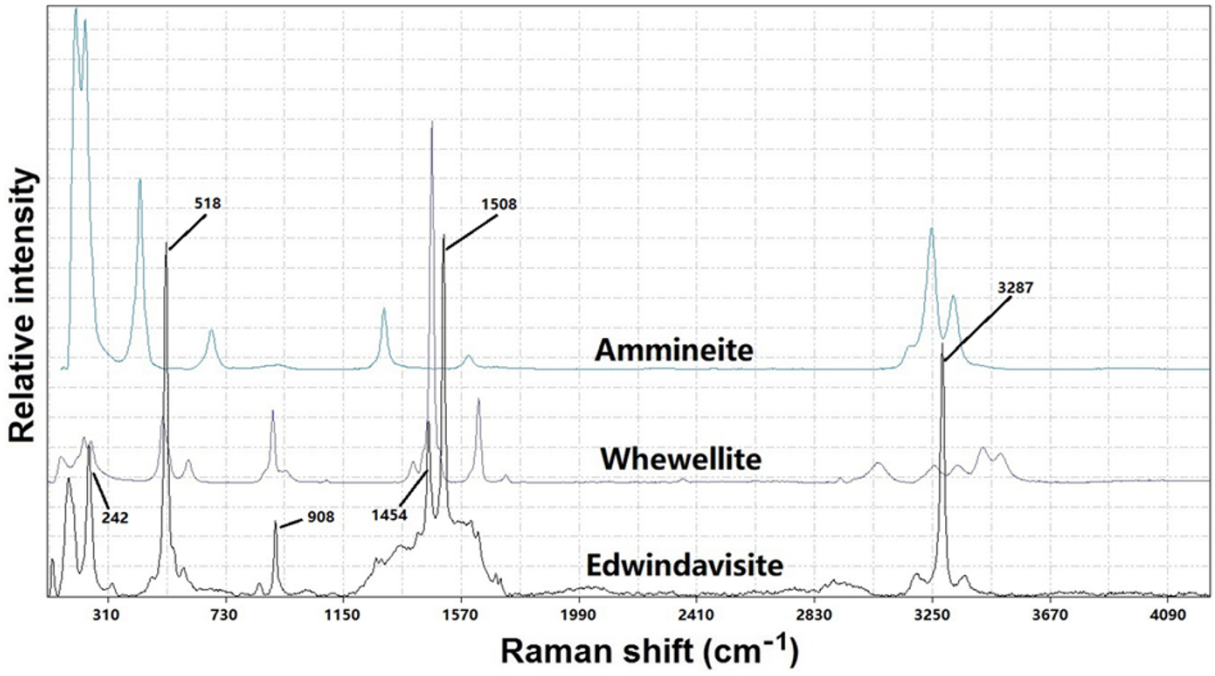

Figure 4. Raman spectra of edwindavisite, whewellite and ammineite.

Sample description and experimental methods

Occurrence

Edwindavisite was discovered on specimens collected on the 125-foot level of the Rowley mine, ~20 km NW of Theba, Maricopa County, Arizona, USA (33°257'N, 113°149.59'W). This mine is a former Cu-Pb-Au-Ag-Mo-V-baryte-fluorspar mine that exploited veins presumed to be related to the intrusion of an andesite porphyry dyke into Tertiary volcanic rocks. The mine has not been operated for ore since 1923, but it has been a rich source of fine wulfenite crystals for mineral collectors in the past 70 years. A detailed description of the history, geology and mineralogy of the Rowley mine has been presented by Wilson (2020). Edwindavisite was found on a quartz matrix, in intimate association with ammineite, a sampleite-like mineral, baryte, ebnerite and wulfenite (Fig. 1). The area where the edwindavisite specimens were collected has an unusual bat guano-related, secondary mineral assemblage, from which a number of new mineral species have been discovered, including rowleyite (Kampf *et al.*, 2017), phoxite (Kampf *et al.*, 2019b), davidbrownite-(NH_4) (Kampf *et al.*, 2019a), natrosulfatourea (Kampf *et al.*, 2021a), allantoin (Kampf *et al.*, 2021a), thebaite-(NH_4) (Kampf *et al.*, 2021b), relianceite-(K) (Kampf *et al.*, 2022a), dendoraite-(NH_4) (Kampf *et al.*, 2022a), ebnerite, epiebnerite (Kampf *et al.* 2024), ferriphoxite and carboferriphoxite (Kampf *et al.*, 2025a).

Appearance, physical and chemical properties

Edwindavisite occurs as radial fans or sprays of bladed or prismatic crystals, elongated on [001]. Individual crystals are up to 0.50 × 0.08 × 0.06 mm (Figs 2 and 3), with the common forms being {100}, {010} and {001}. It is green, transparent with a pale green streak and vitreous lustre. Edwindavisite is brittle and has a Mohs hardness of ~2 (based on scratch tests); cleavage is perfect on {100}. No parting was observed. The density, measured by flotation in heavy liquids, is 2.55(2) g/cm^3 and the calculated density is 2.53 g/cm^3 on the basis of the empirical chemical formula and the unit-cell volume determined from single-crystal X-ray diffraction data. Optically, edwindavisite is biaxial (+), with $\alpha = 1.550(2)$, $\beta = 1.559(2)$, $\gamma = 1.755(5)$ (white light), $2V_{meas.} = 26(2)°$ and $2V_{cal.} = 26.4°$. The dispersion is distinct with $r > v$. The optical orientation is X = **a**, Y = **c**, Z = **b**, and the pleochroism is X = light green, Y = pale green and Z = deep green, with $Y < X \ll Z$. The compatibility index was not calculated, because of the lack of a k-value for the NH_3 group. Based on the measured optical data and density, along with an ideal chemical formula, we derived an estimated k-value of 0.495 for the NH_3 molecule. Given this k-value for NH_3, we obtained a compatibility index of –0.005 (superior) for edwindavisite and –0.018 (superior) for shilovite, $Cu(NH_3)_4(NO_3)_2$, with the data reported by Chukanov *et al.* (2015).

Table 2. Tentative assignments of major Raman bands for edwindavisite

Bands (cm^{-1})	Assignment
3160–3450	N–H stretching modes in NH_3 groups.
1120–1735	C=O and C–O stretching vibrations within the C_2O_4 groups and the H–N–H bending modes within the NH_3 groups.
840–950	C–C stretching vibrations and O–C–O bending modes within the C_2O_4 groups.
440–620	C–C–O bending modes within the C_2O_4 groups and the Cu–O stretching modes involving the shortest Cu–O bonds.
<350	Rotational and translational vibrational modes of C_2O_4 and NH_3 groups, the Cu^{2+}–(O,N) interactions and lattice vibrational modes.

The chemical composition of edwindavisite was determined using a Shimadzu EPMA-1720 electron microprobe (WDS mode, 15 kV, 10 nA and 5 μm beam diameter). The analytical data (average of 7 analysis points) are given in Table 1, along with

https://doi.org/10.1180/mgm.2025.16 Published online by Cambridge University Press

Table 3. Powder X-ray diffraction data (*d* in Å, *I* in %) for edwindavisite

h	*k*	*l*	I_{cal}	I_{meas}	d_{cal}	d_{meas}	*h*	*k*	*l*	I_{cal}	I_{meas}	d_{cal}	d_{meas}
2	0	0	97.8	92	5.601	5.608	5	2	2	9.3	17	1.823	1.820
2	1	0	86.1	82	4.815	4.797	3	4	2	17.4	19	1.801	1.800
0	2	0	20.6	59	4.713	4.679	6	2	0	9.5	12	1.736	1.735
0	0	2	3.9	8	4.202	4.195	1	5	2	8.1	11	1.700	1.700
1	0	2	13.2	17	3.934	3.936	5	3	2	5.6	10	1.673	1.671
1	1	2	100.0	100	3.631	3.623	4	1	4	11.0	14	1.655	1.655
2	0	2	3.3	11	3.361	3.341	3	4	3	0.9	2	1.624	1.626
2	2	1	3.4	5	3.314	3.301	6	3	0	0.7	1	1.605	1.604
3	1	1	12.4	25	3.208	3.203	4	2	4	2.0	3	1.583	1.584
0	2	2	6.1	16	3.136	3.142	0	4	4	1.7	4	1.568	1.568
1	2	2	18.0	19	3.020	3.013	5	0	4	0.6	1	1.533	1.532
3	2	1	2.0	8	2.764	2.771	5	4	2	4.4	7	1.515	1.513
2	3	0	9.6	15	2.740	2.744	7	1	2	4.8	6	1.477	1.478
4	1	0	15.5	13	2.684	2.687	6	4	0	1.4	1	1.463	1.462
1	1	3	12.2	18	2.611	2.614	3	6	1	1.4	4	1.427	1.426
1	3	2	20.4	29	2.455	2.467	6	0	4	2.4	2	1.396	1.396
3	2	2	25.3	45	2.402	2.402	3	6	2	4.9	7	1.369	1.369
4	0	2	4.3	5	2.330	2.342	7	3	2	5.1	4	1.350	1.349
4	2	1	4.5	11	2.314	2.323	6	2	4	3.6	3	1.338	1.339
2	2	3	3.0	5	2.212	2.211	3	0	6	1.7	3	1.311	1.310
2	4	0	1.5	1	2.172	2.172	6	4	3	0.8	1	1.297	1.297
4	3	0	10.5	31	2.091	2.098	1	3	6	4.1	6	1.271	1.271
1	4	2	6.6	11	2.022	2.023	4	5	4	2.3	1	1.254	1.256
2	0	4	5.9	11	1.967	1.967	5	6	2	1.2	1	1.230	1.230
2	1	4	10.8	24	1.926	1.926	4	7	0	1.2	2	1.214	1.213
6	0	0	4.4	6	1.867	1.865							

Table 4. Crystallographic data for natural and synthetic edwindavisite

	Natural	Synthetic
Ideal formula	$Cu(C_2O_4)(NH_3)$	$Cu(C_2O_4)(NH_3)$
Crystal symmetry	Orthorhombic	Orthorhombic
Space group	*Pbca*	*Pbca*
a (Å)	11.1998(10)	11.19(1)
b (Å)	9.4307(9)	9.43(1)
c (Å)	8.3977(7)	8.38(1)
V (Å^3)	886.98(14)	884.27
Z	8	8
ρ_{cal}(g/cm^3)	2.53	2.53
2θ range for data collection (°)	≤ 67.03 (Mo*K*)	≤ 140 (Cu*K*)
No. of reflections collected		7362
No. of independent reflections	1734	840
No. of reflections with $I > 2\sigma(I)$	1306	587
No. of parameters refined		83
Extinction coefficient		0.0022(6)
R(int)		0.032
Final R_1, wR_2 factors [$I > 2\sigma(I)$]	0.028, 0.070	0.050
Goodness-of-fit		1.052
Reference	This study	Cavalca *et al.* (1972)

Table 5. Fractional atom coordinates and isotropic or equivalent isotropic displacement parameters (Å^2) for edwindavisite

Atom	*x/a*	*y/b*	*z/c*	U_{iso}*/U_{eq}
Cu	0.07575(2)	0.23739(2)	0.12329(2)	0.01620(9)
C1	0.01950(16)	0.48530(18)	−0.0871(2)	0.0156(3)
C2	−0.06441(15)	0.02347(19)	0.0145(2)	0.0147(3)
O1	−0.07988(11)	0.14538(14)	0.07128(16)	0.0184(3)
O2	0.06281(14)	0.36702(16)	−0.11676(14)	0.0243(3)
O3	0.14561(12)	0.06211(13)	0.02329(15)	0.0187(3)
O4	0.00332(13)	0.58327(13)	−0.18736(15)	0.0199(3)
N	0.23377(17)	0.3016(2)	0.1954(2)	0.0249(4)
H1	0.268(2)	0.235(3)	0.242(4)	0.050*
H2	0.274(3)	0.343(3)	0.134(3)	0.050*
H3	0.233(2)	0.349(3)	0.272(3)	0.050*

the standards used for the probe analyses. The resultant empirical chemical formula, calculated on the basis of 1 Cu apfu, is $Cu_{1.00}(C_2O_4)(NH_3)_{0.99}$. The hydrogen content was calculated by stoichiometry. The ideal formula, $Cu(C_2O_4)(NH_3)$, requires (wt.%) CuO 47.18, C_2O_3 42.72, NH_3 10.10 (total = 100%). At room temperature, edwindavisite is insoluble in H_2O, but easily soluble in dilute HCl.

Raman spectra

The Raman spectrum of edwindavisite (Fig. 4) was collected from a randomly orientated crystal on a Thermo Almega microRaman system, using a solid-state laser with a frequency of 532 nm at 50 mW power (1/3 of the full power to avoid the burning by the laser) and a thermoelectric cooled CCD detector. The laser is partially polarised with 4 cm^{-1} resolution and a spot size of 1 μm.

The tentative assignments of major Raman bands for edwindavisite were made based on spectroscopic studies on materials containing oxalate $(C_2O_4)^{2-}$ and/or ammine groups, such as synthetic edwindavisite $Cu(C_2O_4)(NH_3)$ (Cavalca *et al.*, 1972), ammineite $CuCl_2(NH_3)_2$ (Bojar *et al.*, 2010), humboldtine $Fe^{2+}(C_2O_4)\cdot 2H_2O$ (Frost and Weier, 2003; Echigo and Kimata, 2008), whewellite $Ca(C_2O_4)\cdot H_2O$ (Shippey, 1980; Frost and

https://doi.org/10.1180/mgm.2025.16 Published online by Cambridge University Press

Table 6. Anisotropic displacement parameters (Å^2) for edwindavisite

Atom	U^{11}	U^{22}	U^{33}	U^{12}	U^{13}	U^{23}
Cu	0.01810(14)	0.01187(12)	0.01863(14)	0.00018(8)	−0.00070(9)	−0.00223(8)
C1	0.0202(9)	0.0130(7)	0.0135(7)	0.0013(6)	0.0002(6)	−0.0013(6)
C2	0.0182(8)	0.0140(7)	0.0120(7)	0.0028(6)	−0.0008(6)	0.0011(6)
O1	0.0190(6)	0.0145(6)	0.0219(6)	0.0032(5)	−0.0015(5)	−0.0053(5)
O2	0.0418(9)	0.0152(6)	0.0159(7)	0.0110(6)	0.0040(6)	−0.0015(5)
O3	0.0177(6)	0.0157(6)	0.0226(6)	−0.0001(5)	−0.0004(5)	−0.0024(5)
O4	0.0324(7)	0.0132(6)	0.0142(6)	0.0029(5)	0.0020(5)	0.0004(5)
N	0.0242(9)	0.0258(9)	0.0247(9)	−0.0089(7)	0.0007(7)	0.0005(7)

Table 7. Selected bond distances (Å) for edwindavisite

	Natural	Synthetic		Natural	Synthetic		Natural	Synthetic
	(This study)	(Cavalca *et al.*, 1972)		(This study)	(Cavalca *et al.*, 1972)		(This study)	(Cavalca *et al.*, 1972)
Cu–N	1.9660(19)	1.988(7)	C1–O2	1.241(2)	1.243(9)	N–H1	0.83(3)	0.91
Cu–O4	1.9835(13)	1.982(5)	C1–O4	1.263(2)	1.277(9)	N–H2	0.79(3)	0.89
Cu–O1	1.9955(13)	1.996(5)	C1–C1	1.552(4)	1.55(2)	N–H3	0.78(3)	0.90
Cu–O3	2.0124(13)	2.011(5)						
Cu–O2	2.3621(13)	2.360(6)	C2–O1	1.257(2)	1.255(9)			
Cu–O2	2.3992(12)	2.391(6)	C2–O3	1.257(2)	1.258(8)			
			C2–C2	1.529(3)	1.53(2)			

Table 8. Hydrogen-bond geometry (Å, °) in edwindavisite

D—H···*A*	*D*—H	H···*A*	*D*···*A*	*D*—H···*A*
N—H1···O1^{v}	0.83(2)	2.46(2)	3.220(2)	151(3)
N—H2···O1^{vi}	0.79(2)	2.38(2)	3.102(2)	153(3)
N—H2···O3^{vii}	0.79(2)	2.44(2)	3.154(2)	151(3)
N—H3···O3^{ii}	0.78(2)	2.47(2)	3.195(2)	154(3)

Notes: Symmetry codes: (ii) x, $-y+½$, $z+½$; (v) $x+½$, y, $-z+½$; (vi) $x+½$, $-y+½$, $-z$; (vii) $-x+½$, $y+½$, z. *D* = donor; *A* = acceptor.

Table 9. Bond-valence sums (vu) for edwindavisite

Atom	Cu	C1	C2	H1	H2	H3	Sum
O1	0.353		1.481	0.090	0.099		2.022
O2	0.131	1.562					1.812
	0.118						
O3	0.337		1.479		0.092	0.088	1.996
O4	0.364	1.448					1.812
N*	0.599			(1.191)	(1.292)	(1.311)	(4.353)
C1		0.970					
C2			1.040				
Sum	1.863	3.980	4.000	(1.281)	(1.483)	(1.399)	

Note: The significant deviation of bond-valence sums from the ideal values for N^{3+} and H^{+} ions is due to the fact that the bond-valence parameters (R_0 = 0.935 Å and B = 0.572 Å) given by Gagné (2021) were derived from the neutron diffraction data based on the average N–H distance of 0.999 Å (with a range of 0.915–1.025 Å). This N–H distance is remarkably longer than any reported N–H distances determined from the X-ray structure analyses for the NH_3 group (0.7–0.9 Å). If we constrain our N–H distance to be 0.95 Å, then we have the bond valence sums of 3.48 vu for N and 0.97 vu for H.

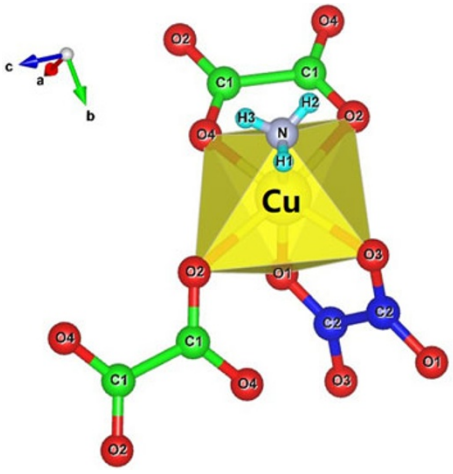

Figure 5. The configuration of the Cu atom coordinated octahedrally by (5O + N) in edwindavisite. The structures were drawn using VESTA (Momma and Izumi, 2011).

Weier, 2003), and shilovite $Cu(NH_3)_4(NO_3)_2$ (Chukanov *et al.*, 2015). Specifically, the Raman spectrum of edwindavisite can be divided into five regions (Table 2). Region 1 ranges from 3160 to 3450 cm^{-1}, with a relatively strong peak centred at 3287 cm^{-1}. The bands in this region are due to the N–H stretching modes in NH_3 groups. Region 2 includes the bands between 1120 and 1735 cm^{-1}, which are ascribable to the C=O and C–O stretching vibrations within the C_2O_4 groups, as well as the H–N–H bending modes within the NH_3 groups. In particular, the two sharp peaks, one at 1508 cm^{-1} and the other at 1454 cm^{-1}, correspond to the symmetric stretching vibrations of C=O and C–O bonds within C_2O_4. It is interesting to note that whewellite only shows one strong peak at 1493 cm^{-1} in this region, whereas both oxammite, $(NH_4)_2(C_2O_4)\cdot H_2O$ and moolooite, $Cu(C_2O_4)\cdot nH_2O$, exhibit two relatively strong peaks (Frost and Weier, 2003). Region 3 spans the region from 840 to 950 cm^{-1}. The sharp peak at 908 cm^{-1} in this region is assigned to the C–C stretching vibrations and the weak bands are attributed to the O–C–O antisymmetric bending modes within the C_2O_4 groups. In comparison, the band corresponding to the C–C stretching vibrations is observed at 909 cm^{-1} for weddellite and 921 cm^{-1} for moolooite (Frost and Weier, 2003). Region 4 ranges from 440 to 620 cm^{-1}. The strong peak at 518 cm^{-1} in the region corresponds to the C–C–O bending

https://doi.org/10.1180/mgm.2025.16 Published online by Cambridge University Press

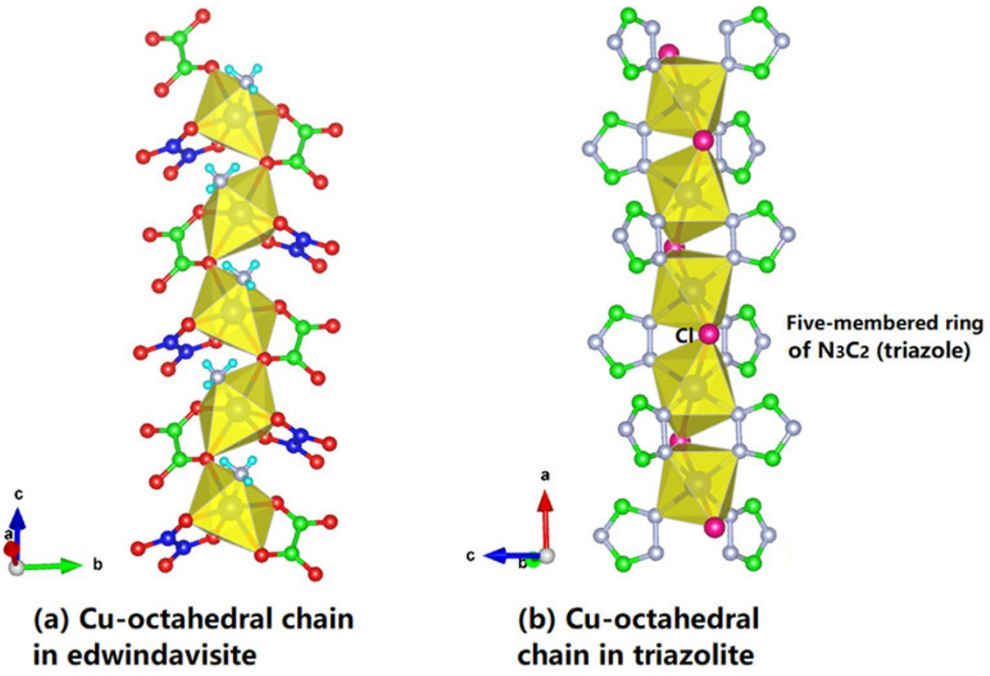

Figure 6. A corner-sharing Cu-octahedral chain in (a) edwindavisite and (b) triazolite.

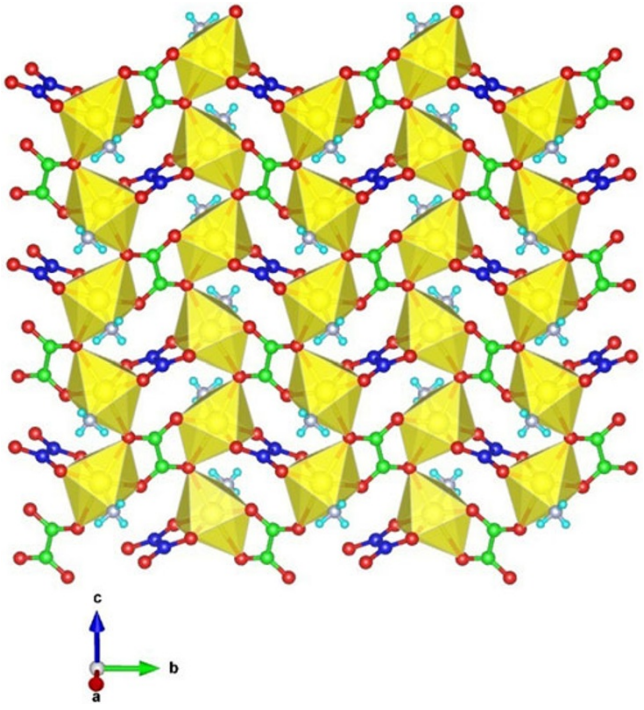

Figure 7. A layer of corner-sharing Cu-octahedral chains linked together by oxalate groups in edwindavisite. The figure legends are the same as in Fig. 5.

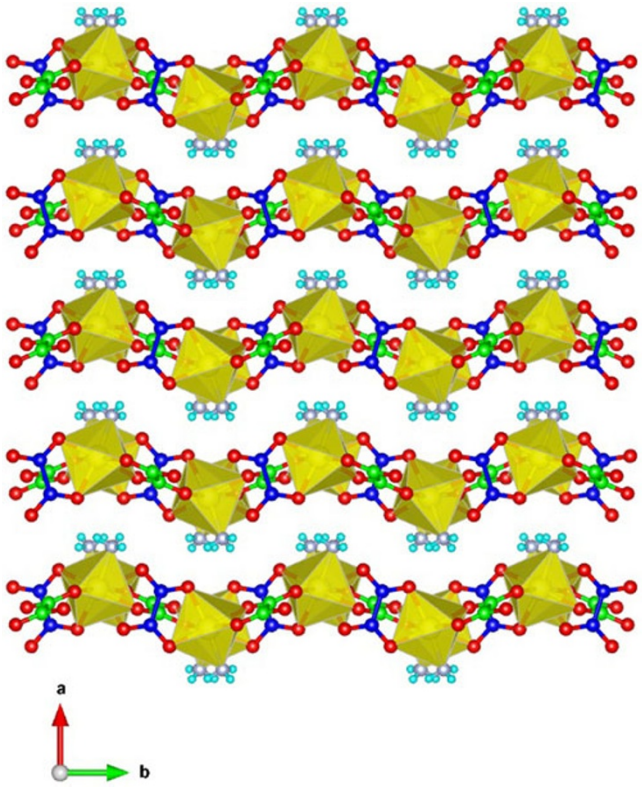

Figure 8. Crystal structure of edwindavisite, showing the $Cu(C_2O_4)(NH_3)$ layers stacked along [100], which are interconnected by N–H···O hydrogen bonds provided by NH_3 ammonia molecules. For clarity and simplicity, N–H···O hydrogen bonds between $Cu(C_2O_4)(NH_3)$ layers are not drawn. The figure legends are the same as in Fig. 5.

https://doi.org/10.1180/mgm.2025.16 Published online by Cambridge University Press

mode and the rest of the bands can be attributed to the Cu–O stretching modes involving the shortest Cu–O bonds. Region 5 includes the bands below 350 cm^{-1}, which are associated mainly with the rotational and translational modes of C_2O_4 and NH_3 groups, as well as the Cu^{2+}–(O,N) interactions and lattice vibrational modes. For comparison, the Raman spectra of ammineite and whewellite from the RRUFF Project (Lafuente *et al.*, 2015) are also plotted in Fig. 4.

X-ray crystallography

Powder X-ray diffraction data for edwindavisite were collected on a Rigaku Xtalab Synerg D/S 4-circle diffractometer equipped with Cu*K* radiation and operated at 50 kV and 1 mA. Powder X-ray diffraction data (Table 3) were collected in the Gandolfi powder mode and the unit-cell parameters refined using the program by Holland and Redfern (1997) are: $a = 11.2011(4)$, $b = 9.4260(3)$, $c = 8.4042(3)$ Å and $V = 887.33(3)$ Å^3.

Single-crystal X-ray diffraction data of edwindavisite were collected on a Bruker APEX2 4-circle diffractometer equipped with Mo*K* radiation from a 0.06 × 0.05 × 0.05 mm fragment. All reflections were indexed on the basis of an orthorhombic unit cell (Table 4). The systematic absences of reflections suggest the unique space group *Pbca*. The structure was solved with *SHELXT* (Sheldrick, 2015a) and refined using *SHELXL2019* (Sheldrick, 2015b). All H atoms were located through the difference-Fourier syntheses. The positions of all atoms were refined with anisotropic displacement parameters, except for H atoms, which were refined with a fixed isotropic displacement parameter ($U_{iso} = 0.05$ Å^2) and soft restraints of 0.85(3) Å on the N–H distances. The final refinement statistics are listed in Table 3. Atomic coordinates and displacement parameters are given in Tables 5 and 6, respectively. Selected bond distances are presented in Table 7 and hydrogen bonding geometries in Table 8. The bond-valence sums (BVS) were calculated using the parameters given by Brown (2009) for Cu–O and Cu–N bonds, Harris and Hardcastle (2015) for C–C and C–O bonds, Gagné (2021) for N–H bonds, and by Ferraris and Ivaldi (1988) for O···H bonds (Table 9). The crystallographic information file has been deposited with the Principal Editor of *Mineralogical Magazine* and is available as Supplementary material (see below).

Crystal structure description and discussion

Edwindavisite is the natural analogue of synthetic *catena*-μ-oxalato-ammine-copper(II), $Cu(C_2O_4)(NH_3)$ (Cavalca *et al.*, 1972) (Table 4). In its structure, each Cu^{2+} cation is coordinated by (5O + N), forming a rather distorted and elongated octahedron (Fig. 5) due to the Jahn-Teller effect. The five O atoms coordinated to a Cu atom are from three different $(C_2O_4)^{2-}$ groups, two being bidentately bonded and one monodentately bonded, with the Cu–O bond lengths ranging from 1.983 to 2.399 Å. The Cu–N distance (1.966 Å) is shorter than any of the Cu–O distances, but agrees well with the values reported for Cu that is bonded to NH_3 (Bojar *et al.*, 2010 and references therein).

The Cu-octahedra in the edwindavisite structure share corners with one another to form chains extending along [001] (Fig. 6), which are joined together by oxalate $(C_2O_4)^{2-}$ groups, giving rise to layers parallel to (100) (Fig. 7). Such layers are interconnected by N–H···O hydrogen bonds (Table 8, Fig. 8). Similar chains of corner-sharing Cu-octahedra have also been observed in triazolite, $NaCu_2(N_3C_2H_2)_2(NH_3)_2Cl_3{\cdot}4H_2O$ (Chukanov *et al.*, 2018) (Fig. 6), and pabellóndepicaite, $Cu^{2+}{}_2(N_3C_2H_2)_2(NH_3)_2(NO_3)Cl{\cdot}2H_2O$ (Kampf *et al.*, 2025b), both being Cu-bearing organic minerals containing 1,2,4-triazolate anions, as well as NH_3 molecules.

Oxalic acid is ubiquitous in natural environments. It can be produced by some plants, fungi and lichens (e.g. Dutton and Evans, 1996; Prieto *et al.*, 1997; Chen *et al.*, 2000; Grąz, 2024). Lichens and fungi living on mineral surfaces have been found to facilitate the dissolution of heavy metals (e.g. Chisholm *et al.*, 1987; Fomina *et al.*, 2005; Studenroth *et al.*, 2013; Schuler *et al.*, 2021; Amenaghawon *et al.*, 2024). Yet, only 37 oxalate minerals have been documented to date. Among them, six contain Cu [antipinite, $KNa_3Cu_2(C_2O_4)_4$, edwindavisite, fiemmeite, $Cu_2(C_2O_4)(OH)_2{\cdot}2H_2O$, middlebackite, $Cu_2C_2O_4(OH)_2$, moolooite, $Cu(C_2O_4){\cdot}nH_2O$, and wheatleyite, $Na_2Cu(C_2O_4)_2{\cdot}2H_2O$], and seven contain ammonium $(NH_4)^+$ [davidbrownite-(NH_4), $(NH_4)_5(V^{4+}O)_2(C_2O_4)[PO_{2.75}(OH)_{1.25}]_4{\cdot}3H_2O$, dendoraite-$(NH_4)$, $(NH_4)_2NaAl(C_2O_4)(PO_3OH)_2(H_2O)_2$, oxammite, $(NH_4)_2(C_2O_4){\cdot}H_2O$, phoxite $(NH_4)_2Mg_2(C_2O_4)(PO_3OH)_2(H_2O)_4$, thebaite-$(NH_4)$, $(NH_4)_3Al(C_2O_4)(PO_3OH)_2(H_2O)$, ferriphoxite, $[(NH_4)_2K(H_2O)][Fe^{3+}(HPO_4)_2(C_2O_4)]$, and carboferriphoxite, $[(NH_4)K(H_2CO_3)][Fe^{3+}(HPO_4)(H_2PO_4)(C_2O_4)]$]. Edwindavisite represents the first oxalate mineral that contains neutral ammonia (NH_3).

Nitrogen is usually present in minerals as $(NO_3)^-$ or $(NH_4)^+$ ionic groups. In the current IMA-approved mineral list (Pasero, 2025), only seven minerals contain the neutral ammonia molecule (NH_3) as a species-defining component: ammineite, $CuCl_2{\cdot}2NH_3$, chanabayaite, $Cu_2Cl(N_3C_2H_2)_2(NH_3,Cl,H_2O,\square)_4$, joanneumite, $Cu(C_3N_3O_3H_2)_2(NH_3)_2$, pabellóndepicaite, $Cu^{2+}{}_2(N_3C_2H_2)_2(NH_3)_2(NO_3)Cl{\cdot}2H_2O$, shilovite, $Cu(NH_3)_4(NO_3)_2$, triazolite, $NaCu_2(N_3C_2H_2)_2(NH_3)_2Cl_3{\cdot}4H_2O$, and edwindavisite. Interestingly, all these minerals have only been described in the past 20 years. Among them, all but edwindavisite were discovered at Pabellón de Pica, Iquique Province, Chile. Moreover, all of them have Cu^{2+} as the essential component and bonded to NH_3. Nonetheless, it is unclear how the presence of Cu^{2+} is related to the formation of NH_3-bearing minerals.

Supplementary material. The supplementary material for this article can be found at https://doi.org/10.1180/mgm.2025.16

Acknowledgements. We are very grateful to Prof Peter Leverett and two anonymous reviewers for their constructive comments.

Competing interests. The authors declare none.

References

Aimable A., Puentes A.T. and Bowen P. (2011) Synthesis of porous and nanostructured particles of CuO via a copper oxalate route. *Powder Technology*, **208**, 467–471.

Amenaghawon A.N., Ayere J.E., Amune U.O., Otuya I.C., Abuga E.C. Anyalewechi C.L. and Darmokoesoemo H. (2024) A comprehensive review of recent advances in the applications and biosynthesis of oxalic acid from bio-derived substrates. *Environmental Research*, **251**, 118703.

Androš L., Jurić M., Planinić P., Žilić D., Rakvin B. and Molčanov K. (2010) New mononuclear oxalate complexes of copper (II) with 2D and 3D architectures: Synthesis, crystal structures and spectroscopic characterization. *Polyhedron*, **29**, 1291–1298.

Baran E.J. (2014) Natural oxalates and their analogous synthetic complexes. *Journal of Coordination Chemistry*, **67**, 3734–3768.

Baran E.J. and Monje P.V. (2008) Oxalate biominerals. *Biomineralization: From Nature to Application*, **4**, 219–254.

Behnoudnia F. and Dehghani H. (2013) Copper (II) oxalate nanospheres and its usage in preparation of $Cu(OH)_2$, Cu_2O and CuO nanostructures: Synthesis and growth mechanism. *Polyhedron*, **56**, 102–108.

Bojar H.P., Walter F., Baumgartner J. and Färber G. (2010) Ammineite, $CuCl_2(NH_3)_2$, a new species containing an ammine complex: Mineral data and crystal structure. *The Canadian Mineralogist*, **48**, 1359–1371.

Brown I.D. (2009) Recent developments in the methods and applications of the bond valence model. *Chemical Reviews*, **109**, 6858–6919.

Cavalca L., Villa A.C., Manfredotti A.G., Mangia A. and Tomlinson A.A.G. (1972) Crystal, molecular and electronic structure of catena-μ-oxalato-ammine-copper (II). *Journal of the Chemical Society Dalton Transactions*, **3**, 391–395.

Chen J., Blume H.P. and Beyer L. (2000) Weathering of rocks induced by lichen colonization—a review. *Catena*, **39**, 121–146.

Chisholm J.E., Jones G.C. and Purvis O.W. (1987) Hydrated copper oxalate, moolooite, in lichens. *Mineralogical Magazine*, **51**, 715–718.

Chukanov N.V., Britvin S.N., Möhn G., Pekov I.V., Zubkova N.V., Nestola F., Kasatkin A.V. and Dini M. (2015) Shilovite, natural copper(II) tetrammine nitrate, a new mineral species. *Mineralogical Magazine*, **79**, 613–623.

Chukanov N.V., Zubkova N.V., Möhn G., Pekov I.V., Belakovskiy D.I., Van K.V. and Pushcharovsky D.Y. (2018) Triazolite, $NaCu_2(N_3C_2H_2)_2(NH_3)_2Cl_3{\cdot}4H_2O$, a new mineral species containing 1, 2, 4-triazolate anion, from a guano deposit at Pabellón de Pica, Iquique Province, Chile. *Mineralogical Magazine*, **82**, 1007–1014.

de Faria D.M., Yoshida M.I., Pinheiro C.B., Guedes K.J., Krambrock K., Diniz R. and Machado F.C. (2007) Preparation, crystal structures and spectroscopic characterization of oxalate copper (II) complexes containing the nitrogen ligands 4, 4-dimethyl-2, 2-bipyridine and di (2-pyridyl) sulfide. *Polyhedron*, **26**, 4525–4532.

Donkova B. and Mehandjiev D. (2005) Review Thermal—Magnetic investigation of the decomposition of copper oxalate—A precursor for catalysts. *Journal of Materials Science*, **40**, 3881–3886.

Dutton M.V. and Evans C.S. (1996) Oxalate production by fungi: its role in pathogenicity and ecology in the soil environment. *Canadian Journal of Microbiology*, **42**, 881–895.

Echigo T. and Kimata M. (2008) Single-crystal X-ray diffraction and spectroscopic studies on humboldtine and lindbergite: weak Jahn-Teller effect of Fe^{2+} ion. *Physics and Chemistry of Minerals*, **35**, 467–475.

Ferraris G. and Ivaldi G. (1988) Bond valence vs bond length in O··· O hydrogen bonds. *Acta Crystallographica*, **B44**, 341–344.

Fomina M., Hillier S., Charnock J.M., Melville K., Alexander I.J. and Gadd G.M. (2005) Role of oxalic acid overexcretion in transformations of toxic metal minerals by Beauveria caledonica. *Applied and Environmental Microbiology*, **71**, 371–381.

Frank-Kamenetskaya O.V., Zelenskaya M.S., Izatulina A.R., Vereshchagin O.S., Vlasov D.Y., Himelbrant D.E. and Pankin D.V. (2021) Copper oxalate formation by lichens and fungi. *Scientific Reports*, **11**, 24239.

Frank-Kamenetskaya O., Zelenskaya M., Izatulina A., Gurzhiy V., Rusakov A. and Vlasov D. (2022) Oxalate formation by Aspergillus niger on minerals of manganese ores. *American Mineralogist*, **107**, 100–109.

Frost R.L. and Weier M.L. (2003) Raman spectroscopy of natural oxalates at 298 and 77 K. *Journal of Raman Spectroscopy*, **34**, 776–785.

Furukawa H., Cordova K.E., O'Keeffe M. and Yaghi O.M. (2013) The chemistry and applications of metal-organic frameworks. *Science*, **341**, 1230444.

Gadd G.M., Bahri-Esfahani J., Li Q., Rhee Y.J., Wei Z., Fomina M. and Liang X. (2014) Oxalate production by fungi: significance in geomycology, biodeterioration and bioremediation. *Fungal Biology Reviews*, **28**, 36–55.

Gagné O.C. (2021) On the crystal chemistry of inorganic nitrides: crystal-chemical parameters, bonding behavior, and opportunities in the exploration of their compositional space. *Chemical Science*, **12**, 4599–4622.

Garcia-Teran J.P., Beobide G., Castillo O., Cepeda J., Luque A., Perez-Yanez S. and Roman P. (2019) Supramolecular architectures of metal-oxalato coordination polymers bearing N-tethered adenine nucleobases. *Polyhedron*, **171**, 53–64.

Glukhova L.B., Frank Y.A., Danilova E.V., Avakyan M.R., Banks D., Tuovinen O.H. and Karnachuk O.V. (2018) Isolation, characterization, and metal response of novel, acid-tolerant Penicillium spp. from extremely metal-rich waters at a mining site in Transbaikal (Siberia, Russia). *Microbial Ecology*, **76**, 911–924.

Grąz M. (2024) Role of oxalic acid in fungal and bacterial metabolism and its biotechnological potential. *World Journal of Microbiology and Biotechnology*, **40**, 178 (1–11).

Harris C. and Hardcastle F.D. (2015) Bond length-bond valence relationships for carbon-carbon and carbon-oxygen bonds. *Journal of the Arkansas Academy of Science*, **69**, 45–53.

Hazen R.M., Downs R.T., Jones A.P. and Kah L. (2013) Carbon mineralogy and crystal chemistry. *Reviews in Mineralogy and Geochemistry*, **75**, 7–46.

Hofmann B.A. and Bernasconi S.M. (1998) Review of occurrences and carbon isotope geochemistry of oxalate minerals: implications for the origin and fate of oxalate in diagenetic and hydrothermal fluids. *Chemical Geology*, **149**, 127–146.

Holland T.J.B. and Redfern S.A.T. (1997) Unit cell refinement from powder diffraction data: the use of regression diagnostics. *Mineralogical Magazine*, **61**, 65–77.

Kampf A.R., CooperM.A., Nash B.P., Cerling T., Marty J., Hummer D.R., Celestian A.J., Rose T.P. and Trebisky T.J. (2017) Rowleyite, $[Na(NH_4,K)_9Cl_4][V^{5+,4+}{}_2(P,As)O_8]_6 \cdot n,[H_2O,Na,NH_4,K,Cl]$, a new mineral with a mesoporous framework structure. *American Mineralogist*, **102**, 1037–1044.

Kampf A.R., Cooper M.A., Rossman G.R., Nash B.P., Hawthorne F.C. and Marty J. (2019a) Davidbrownite-(NH_4), $(NH_4,K)_5(V^{4+}O)_2(C_2O_4)[PO_{2.75}(OH)_{1.25}]_4{\cdot}3H_2O$, a new phosphate-oxalate mineral from the Rowley mine, Arizona, USA. *Mineralogical Magazine*, **84**, 869–877.

Kampf A.R., Celestian A.J., Nash B.P. and Marty J. (2019b) Phoxite, $(NH_4)_2Mg_2(C_2O_4)(PO_3OH)_2(H_2O)_4$, the first phosphate-oxalate mineral. *American Mineralogist*, **103**, 973–979.

Kampf A.R., Celestian A.J., Nash B.P. and Marty J. (2021a) Allantoin and natrosulfatourea, two new bat-guano minerals from the Rowley mine, Maricopa County, Arizona, U.S.A. *The Canadian Mineralogist*, **59**, 603–616.

Kampf A.R., Cooper M.A., Celestian A.J., Nash B.P. and Marty J. (2021b) Thebaite-(NH_4), $(NH_4,K)_3Al(C_2O_4)(PO_3OH)_2(H_2O)$, a new phosphate-oxalate mineral from the Rowley mine, Arizona, USA. *Mineralogical Magazine*, **85**, 379–386.

Kampf A.R., Cooper M.A., Celestian A.J., Ma C. and Marty J. (2022a) Dendoraite-(NH_4), a new phosphate-oxalate mineral related to thebaite-(NH_4) from the Rowley mine, Arizona, USA. *Mineralogical Magazine*, **86**, 531–538.

Kampf A.R., Cooper M.A., Celestian A.J., Ma C. and Marty J. (2022b) Relianceite-(K), a new phosphate-oxalate mineral related to davidbrownite-(NH_4) from the Rowley mine, Arizona USA. *Mineralogical Magazine*, **86**, 539–547.

Kampf A.R., Gu X., Yang H., Ma C. and Marty J. (2024) Ebnerite and epiebnerite: NH_4ZnPO_4 dimorphs with zeolite-type frameworks from the Rowley mine Arizona USA. *Mineralogical Magazine*, **88**, 312–318.

Kampf A.R., Ma C., Hawthorne F.C. and Marty J. (2025a) Ferriphoxite and carboferriphoxite: two new oxalato-phosphate minerals from the Rowley mine, Arizona, USA. *Mineralogical Magazine*, **89**, 162–171. doi: 10.1180/mgm.2024.56.

Kampf A.R., Möhn G., Ma C. and Désor J. (2025b) Pabellóndepicaite, $Cu^{2+}_2(N_3C_2H_2)_2(NH_3)_2(NO_3)Cl{\cdot}2H_2O$, a new triazole mineral from the guano deposit at Pabellón de Pica, Iquique Province, Chile. *Mineralogical Magazine*, **89**, 141–147. doi: 10.1180/mgm.2024.55.

Lafuente B., Downs R.T., Yang H., Stone N., Armbruster T. and Danisi R.M. (2015) The power of databases: the RRUFF project. *Highlights in Mineralogical Crystallography*, **1**, 25.

Momma K. and Izumi F. (2011) VESTA 3 for three-dimensional visualization of crystal, volumetric and morphology data. *Journal of Applied Crystallography*, **44**, 1272–1276.

Pasero M. (2025) *The New IMA List of Minerals*. International Mineralogical Association. Commission on new minerals, nomenclature and classification (IMA-CNMNC). http://cnmnc.units.it/

Prieto B., Silva B., Rivas T., Wierzchos J. and Ascaso C. (1997) Mineralogical transformation and neoformation in granite caused by the lichens

https://doi.org/10.1180/mgm.2025.16 Published online by Cambridge University Press

Tephromela atra and Ochrolechia parella. *International Biodeterioration and Biodegradation*, **40**, 191–199.

Ren W.X., Li P.J., Geng Y. and Li X.J. (2009) Biological leaching of heavy metals from a contaminated soil by Aspergillus niger. *Journal of Hazardous Materials*, **167**, 164–169.

Schuler E., Demetriou M., Shiju N.R. and Gruter G.J.M. (2021) Towards sustainable oxalic acid from CO_2 and biomass. *ChemSusChem*, **14**, 3636–3664.

Sheldrick G.M. (2015a) SHELXT – Integrated space-group and crystal structure determination. *Acta Crystallographica*, **A71**, 3–8.

Sheldrick G.M. (2015b) Crystal structure refinement with SHELX. *Acta Crystallographica*, **C71**, 3–8.

Shippey T.A. (1980) Vibrational studies of calcium oxalate monohydrate (whewellite) and an anhydrous phase of calcium oxalate. *Journal of Molecular Structure*, **63**, 157–166.

Singh G., Kapoor I.P.S., Dubey R. and Srivastava P. (2012) Preparation, characterization and catalytic effects of copper oxalate nanocrystals. *Journal of Alloys and Compounds*, **513**, 499–505.

Studenroth S., Huber S.G., Kotte K. and Schöler H.F. (2013) Natural abiotic formation of oxalic acid in soils: results from aromatic model compounds and soil samples. *Environmental Science & Technology*, **47**, 1323–1329.

Tsekova K., Todorova D. and Ganeva S. (2010) Removal of heavy metals from industrial wastewater by free and immobilized cells of Aspergillus niger. *International Biodeterioration & Biodegradation*, **64**, 447–451.

Wilson W.E. (2020) The Rowley mine, Painted Rock Mountains, Maricopa County, Arizona. *Mineralogical Record*, **51**, 181–226.

Wu J.Y. and Huang K. (2016) Precipitation of flaky moolooite and its thermal decomposition. *International Journal of Minerals Metallurgy and Materials*, **23**, 976–980.

Yang H., Gu X., Kampf A.R., Marty J., Gibbs R.B. and Downs R.T. (2023) Edwindavisite, IMA 2023-056. CNMNC Newsletter 75. *Mineralogical Magazine*, **87**, https://doi.org/10.1180/mgm.2023.76

Zelenskaya M.S., Izatulina A.R., Frank-Kamenetskaya O.V. and Vlasov D.Y. (2021) Iron oxalate humboldtine crystallization by fungus Aspergillus niger. *Crystals*, **11**, 1591.

https://doi.org/10.1180/mgm.2025.16 Published online by Cambridge University Press